Electronic Supplementary Information (ESI)

# Supplementary Information

## Decoding the Mechanism of Self-discharge and Optimal Electrolyte Reconfiguration for Advanced Vanadium-based Aqueous Zinc Batteries

Jie Sun[a], Jin Zhang[a], Siyang Wang[b], Peiyan Sun[a], Jiahang Chen[c], Yuping Du[d], Shenghan Wang[a], Ismael Saadoune[e], Yizhan Wang[a], YingjinWei[a*]

[a] Key Laboratory of Physics and Technology for Advanced Batteries (Ministry of Education), College of Physics, Jilin University, Changchun 130012, China.

[b] Department of Chemistry, School of Science, Tianjin Key Laboratory of Molecular Optoelectronic Science, Tianjin University, Tianjin, 300072, China.

[c] College of Chemistry, Jilin University, Changchun, 130012, China.

[d] School of Chemical Engineering, Sichuan University, Chengdu 610065, P. R. China.

[e] Applied Chemistry and Engineering Research Centre of Excellence, Mohammed VI Polytechnic University, Ben Guerir, Morocco.

* yjwei@jlu.edu.cn (Y. Wei)

## Experimental Section

### Synthesis of cathode materials.

0.72 g $V_2O_5$ (Aladdin, 99.5%) were dissolved in 50 mL of deionized water with added 8 mL $H_2O_2$ (Aladdin, 30wt%), and the solution was mixed until it reached a homogeneous dark red appearance without any visible bubbles. The resulting solution was transferred into a 100 mL Teflon-lined stainless-steel autoclave and heated at 200 °C for 4 h. The $V_2O_5 \cdot nH_2O$ were prepared by freeze-drying the hydrogel for 48 h.

### Synthesis and preparation of electrolytes.

The $ZnSO_4$ electrolytes were prepared by dissolving $ZnSO_4 \cdot 7H_2O$ (Sigma-Aldrich, 99%) in deionized water. The $Zn(OTf)_2$ electrolytes were prepared by dissolving $Zn(OTf)_2$ (Damas-Beta, 99%) in deionized water.

The $ZnSO_4$ electrolytes of pH = 3.0, 2.0, and 1.0 were prepared by dissolving pH = 1 $H_2SO_4$ (Aladdin, 37 wt%) into 2 M $ZnSO_4$ (pH = 4.2). This process ignores the effect of volume changes since a relatively smaller volume of $H_2SO_4$ can be introduced to achieve the purpose.

The 2 M $ZnSO_4$−xDMSO−(1-x)$H_2O$ were prepared by dissolving 2 M $ZnSO_4$ into dimethyl sulfoxide (DMSO, Innochem, 99.8%): $H_2O$ with a weight ratio of x: (1-x) (x = 10%, 20%, 30%, 40%, and 50%, respectively).

The 2 M $ZnSO_4$−xEG−(1-x) $H_2O$ were prepared by dissolving 2 M $ZnSO_4$ into ethylene glycol (EG, Chemical Reagent, AR): $H_2O$ with a weight ratio of x: (1-x) (x = 10%, 20%, 30%, 40%, 50%, 60%, 70% and 80%, respectively).

The 2 M $ZnSO_4$-PAM was prepared by dissolving 2 g acrylamide (AM, Aladdin, M.W. ~ 71.08) into 2 mL 2 M $ZnSO_4$. After thorough mixing, 2 mg of N, N'-Methylenebisacrylamide (99.9%, Innochem), and 5 mg of $K_2S_2O_8$ (Macklin, M.W. ~ 270.32) were added and stirred at 40 °C for 30 min. Oxygen was removed using ultrasonication, and the mixture was poured into molds at 60 °C for 30 min. After polymerization, the samples were immersed in 2 M $ZnSO_4$ for ~ 24 h.

The 2 M $ZnSO_4$-40% DMSO-60% $H_2O$-PAM (weight content) was prepared by dissolving 2 M $ZnSO_4$ into DMSO: $H_2O$ with a weight ratio of 2: 3. Then 1 g acrylamide was dissolved into the mixed solution. After thorough mixing, 2 mg of N, N'-Methylenebisacrylamide, and 5 mg of $K_2S_2O_8$ were added and stirred at 40 °C for 30 min. Oxygen was removed using ultrasonication, and the mixture was poured into molds at 60 °C for 40 min. After polymerization, the samples were immersed in 2 M $ZnSO_4$-40% DMSO-60% $H_2O$ for ~ 24 h.

The 2 M $ZnSO_4$-70% EG-30% $H_2O$-PAM (weight content) was prepared by dissolving 2 M $ZnSO_4$ into EG: $H_2O$ with a weight ratio of 7:3. Then 2 g acrylamide was dissolved into the mixed solution. After thorough mixing, 2 mg of N, N'-Methylenebisacrylamide, and 5 mg of $K_2S_2O_8$ were added and stirred at 40 °C for 30 min. Oxygen was removed using ultrasonication, and the mixture was poured into molds at 60 °C for 25 min. After polymerization, the samples were immersed in 2 M $ZnSO_4$-70% EG-30% $H_2O$ for ~ 24 h.

The PAM-40DMSO and PAM-70EG electrolytes, each with a diameter of 11 mm and thickness of 0.7 mm, were used directly without additional separators. The weights of PAM-40DMSO and PAM-70EG were 102 and 101 mg, respectively, comparable to 80 μL of $ZnSO_4$ and $Zn(OTf)_2$ with a weight of 100 and 110 mg, respectively.

**Different anode preparation**

Normal zinc metal was prepared with 6.5 μm-granule sandpaper and smooth zinc metal was prepared with 0.13 μm-granule sandpaper.

## Materials characterizations

X-ray diffraction (XRD) patterns were collected on a SmartLab SE X-ray diffractometer (Rigaku, Japan) with Cu-Kα radiation. Field emission scanning electron microscopy (FE-SEM) and corresponding energy dispersive X-ray spectrometer (EDS) elemental maps were taken by Hitachi Regulus8100 (Hitachi, Japan). Thermogravimetric analysis (TGA) was collected by thermal gravimetric analyzer (TGA Q500 V20.13 Build 39) under argon atmosphere with a heating rate of 10 °C $min^{-1}$ to analyze the structural water content of $V_2O_5 \cdot nH_2O$. Raman spectra were tested with Renishaw InVia Raman spectrometer under excitation with 514 nm radiation. X-ray photoelectron spectroscopy (XPS) was performed using a Thermo SCIENTIFIC ESCALAB 250Xi.

## Electrochemical measurements

To prepare the cathode, $V_2O_5 \cdot nH_2O$: Super P: PVDF = 7: 2: 1, the mixture was coated on Ti foil (10 μm), and dried in a vacuum oven at 60 °C overnight. The Zn||$V_2O_5 \cdot nH_2O$ batteries were assembled into CR2032 coin cells using a 10 mm diameter Zn foil as the anode, $V_2O_5 \cdot nH_2O$ as the cathode, and a glass fiber filter (Whatman GF/C) as the separator. Galvanostatic charge/discharge cycling was investigated using a LAND-2010 automatic battery tester. The float charge current test was set up to detect the change in current by holding the voltage constant at 1.6 V after two pre-cycles. Voltage quantization detection included working electrode $V_2O_5 \cdot nH_2O$, counter electrode Zn, reference electrode Ag/AgCl, exerting current on the working electrode and counter electrode, detecting three types of voltage conditions respectively: (a) working electrode and counter electrode. (b) working electrode and reference electrode. (c) reference electrode and counter electrode. Cyclic

voltammetry (CV), electrochemical impedance spectroscopy (EIS), linear sweep voltammetry (LSV), and Tafel data of the batteries were recorded on a VMP3 (BioLogic, France) electrochemical workstation. CV measurements were performed in the voltage range of 0.2 V to 1.6 V with a scan rate of 0.1 $mV \cdot s^{-1}$. EIS was carried out in the frequency range from 0.01 Hz to $10^5$ Hz. LSV was conducted at a scan rate of 1.0 mV $s^{-1}$. Tafel was performed in the voltage range from −0.25 V to 0.25 V vs. $Zn^{2+}/Zn$.

### *In-situ* pH test

To monitor *in-situ* pH changes, the $V_2O_5 \cdot nH_2O$ cathode and Zn anode were cut into 3.5×3 size with tabs. These electrode films were placed at the two ends of an H-shaped container, with their tabs left for connection to the power lines. In the middle of the H-shaped container, a separator was placed to separate the cathode and anode compartments. A 2 M $ZnSO_4$ electrolyte was then added to the container. Two pH monitoring devices (METTLER TOLEDO, FiveEasy Plus FE28-Standard pH Device) are inserted into each compartment of the container, respectively. The setup was ready for testing, including charging, discharging, and self-discharge experiments. Throughout the testing process, pH values were recorded at regular intervals of every 2 min.

### COMSOL Simulation

All finite-element simulations were calculated and solved using the COMSOL Multiphysics 5.6 software. Surface electric fields of the anodes, cathodes, and zinc sulfate electrolyte internal electric field are calculated using Maxwell's equations. The two-dimensional discrete model was used to investigate the potential distributions and ionic diffusion and accumulation near the anodes and cathodes in the zinc sulfate electrolyte. The flux of $SO_4^{2-}$ anions at the interface region was calculated using the Nernst-Planck equation with diffusion and migration terms. To enhance the

precision of simulating the experimental process, we incorporated the variable potential of the positive electrode employed in the *in-situ* Raman spectroscopy test into the positive electrode material aspect of the model. However, this model and the results of the simulation can reflect only the ideal situation, and does not fully reflect the actual situation.

**Density Functional Theory (DFT) Calculation**

DFT calculations were performed using the Vienna Ab initio simulation package (VASP)[1]. The generalized gradient approximation (GGA) with a Perdew–Burke–Ernzerhof (PBE) exchange–correlation energy was employed[2]. To ensure the convergence criteria of optimization for all structures, a cutoff energy of 400 eV was used for the plane wave basis set along with the projector augmented wave (PAW) method[3], an energy relaxation of $1 \times 10^{-5}$ eV per atom, and a force relaxation of 0.01 eV $Å^{-1}$ was employed. Brillouin zone sampling was conducted using the Monkhorst-Pack scheme, and K-points were generated with VASPkit[4]. A semiempirical DFT-D3 force-field approach was used to include the physical van der Waals (vdW) interaction in our calculations[5]. Adsorption energy calculations were based on the equation: $E_{ad} = E_{total} - E_{slab} - E_{(M)}$, where $E_{total}$ is the total energy of the adsorbed state of DMSO, EG or $H_2O$, $E_{slab}$ is the energy of the $V_2O_5 \cdot H_2O$ (001) surface or the energy of Zn (002), and $E_{(M)}$ is the energy of DMSO, EG or H2O. The vacuum space of 30 Å was adopted to avoid the interaction between the bounding layers.

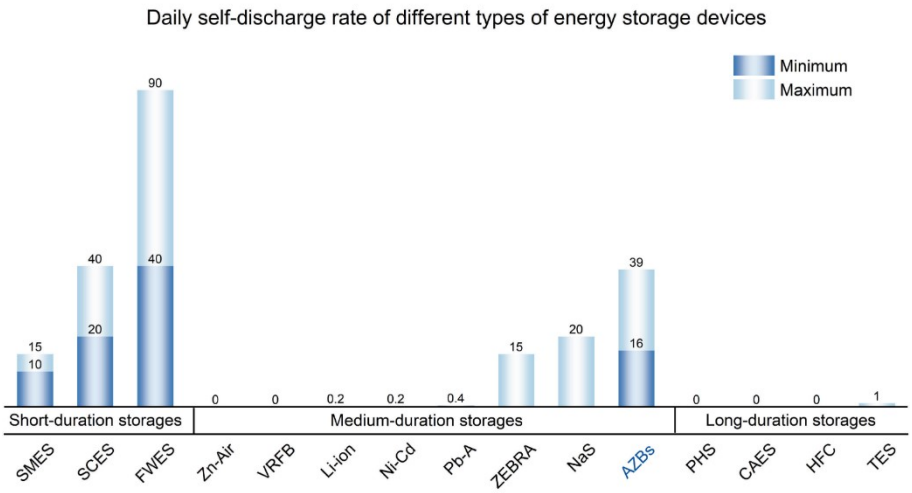


**Fig. S1. Daily self-discharge rate of different types of energy storage devices[6*].**

**Notes*:** The AZBs' data were taken from the experimental 2 M $ZnSO_4$ and $Zn(OTf)_2$ test results in this paper as a comparative reference.

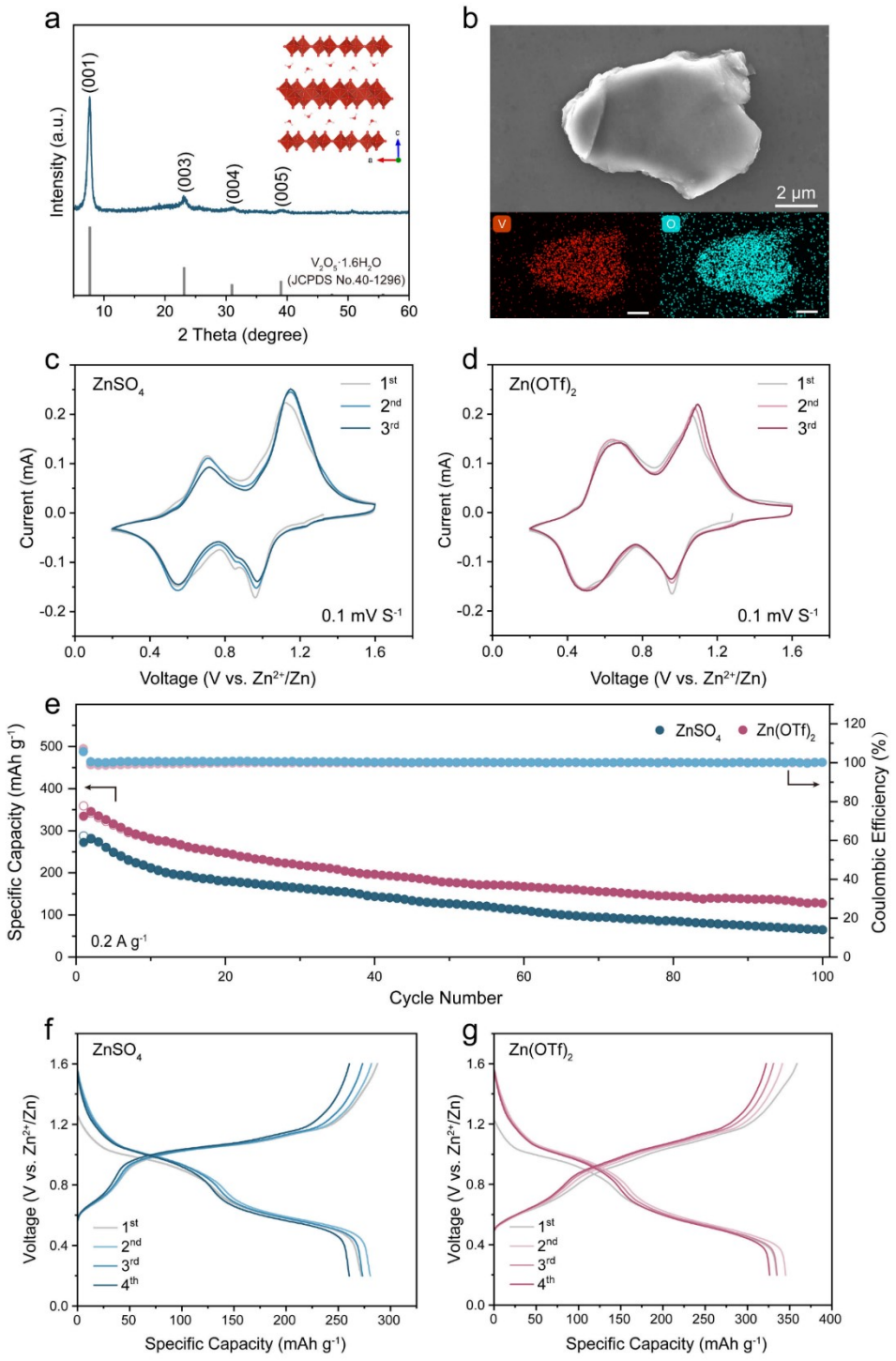


**Fig. S2. Characterizations and electrochemical testing of $V_2O_5 \cdot nH_2O$ materials.** (a) XRD pattern. (b) SEM and EDX elemental maps. (c-d) CV curves at 0.1 mV $s^{-1}$. (e) Cyclic performance at 0.2 A $g^{-1}$. (f-g) Galvanostatic charge-discharge profiles at 0.2 A $g^{-1}$.

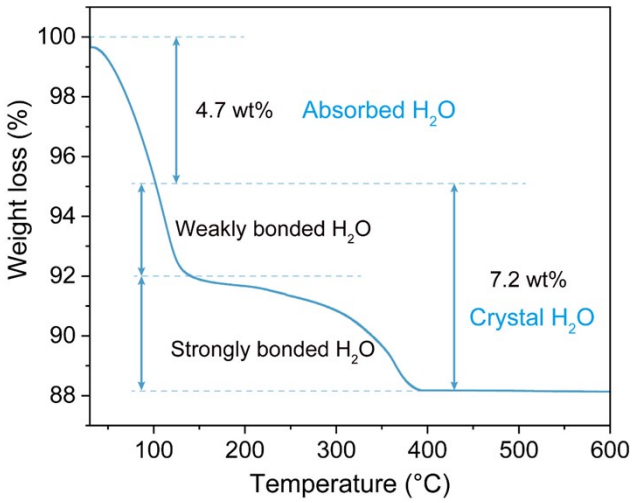


**Fig. S3.** TGA curve of the $V_2O_5 \cdot nH_2O$ material, based on which the water content in the material is determined as 7.2 wt%[7].

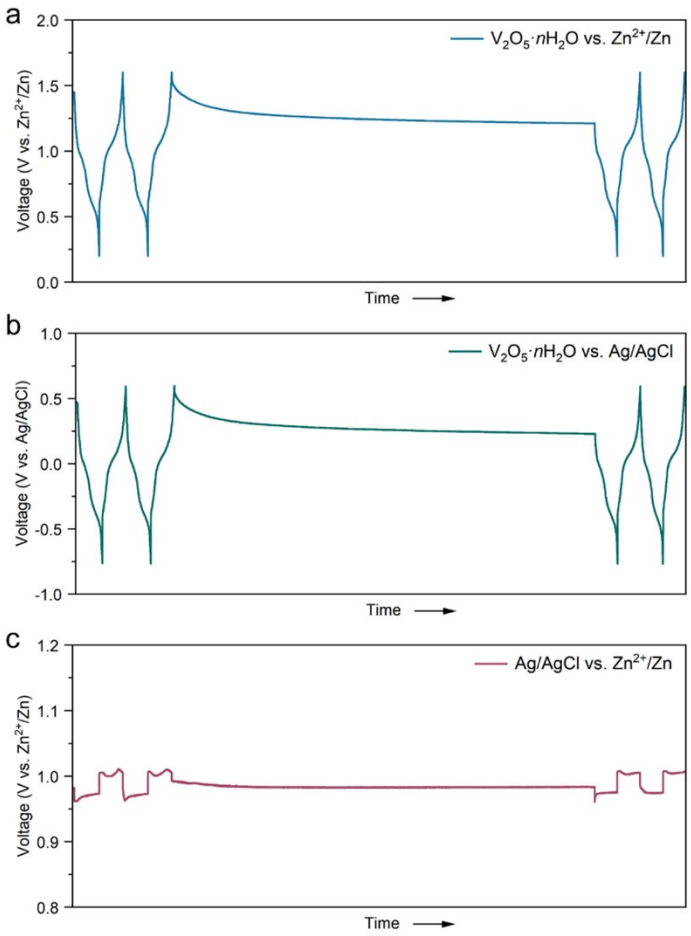


**Fig. S4. Probing the magnitude of self-discharge in voltage on the cathode and anode, respectively.** (a) Cathode vs. Anode: $V_2O_5 \cdot nH_2O$ vs. $Zn^{2+}/Zn$; (b) Cathode vs. Reference electrode: $V_2O_5 \cdot nH_2O$ vs. Ag/AgCl; (c) Reference electrode vs. Anode: Ag/AgCl vs. $Zn^{2+}/Zn$.

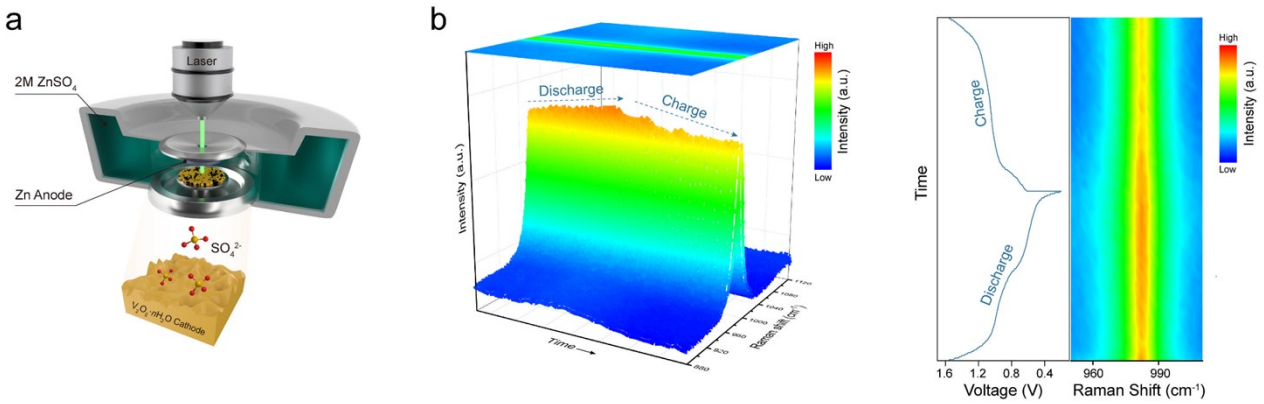


**Fig. S5. *In-situ* Raman on the variation of *v*-$SO_4^{2-}$ on the cathode side throughout the charge/discharge process.** (a) Schematic diagram of *in-situ* Raman device, (b) *In-situ* surface Raman of the $V_2O_5 \cdot nH_2O$ cathode during 2nd cycle of discharge/charge.

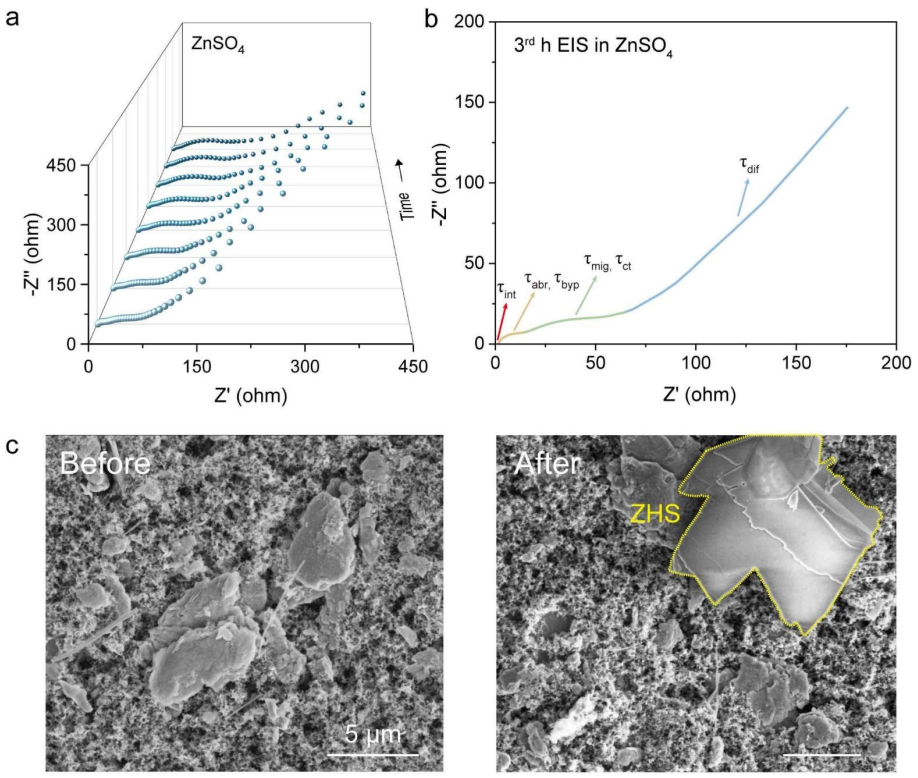


**Fig. S6. *In-situ* EIS testing during self-discharge.** (a) EIS test for every 3 hours during self-discharge. (b) Correspondence between EIS spectrum and DRT spectrum. (c) SEM of cathode surface before and after self-discharge*.

**Notes*:** $Zn_4SO_4(OH)_6{\cdot}nH_2O$ (ZHS): $4Zn^{2+} + SO_4^{2-} + 6OH^- + nH_2O \rightarrow Zn_4SO_4(OH)_6 \cdot nH_2O$ [8, 9]

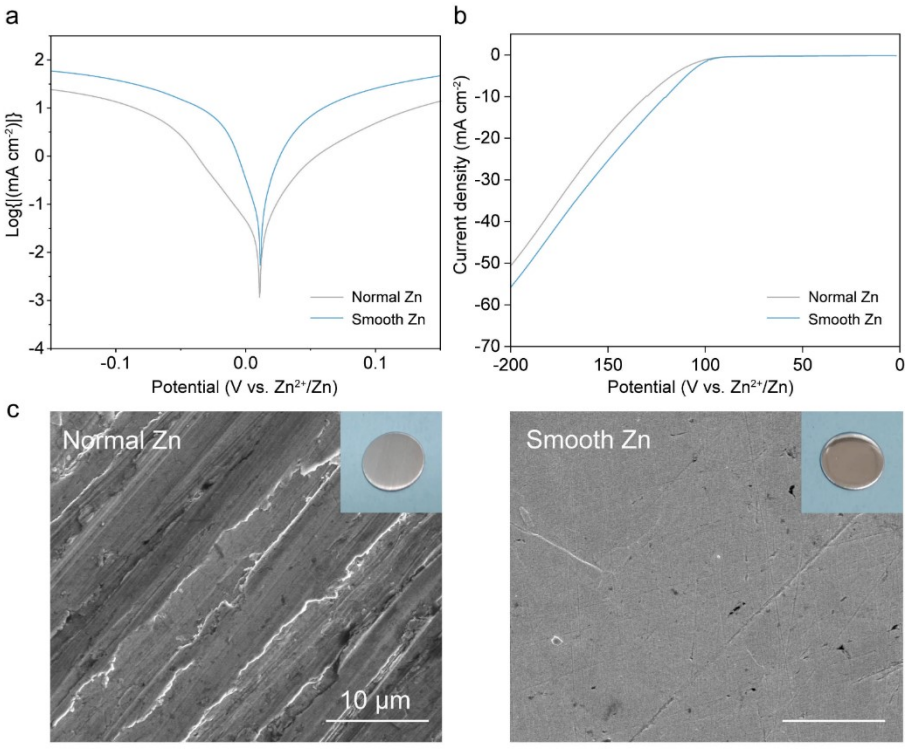


**Fig. S7. Corrosion of Zn with different surface morphology[10].** (a) Tafel curves for normal and smooth Zn. (b) LSV curves for normal and smooth Zn. (c) Optical and SEM morphology of normal and smooth Zn.

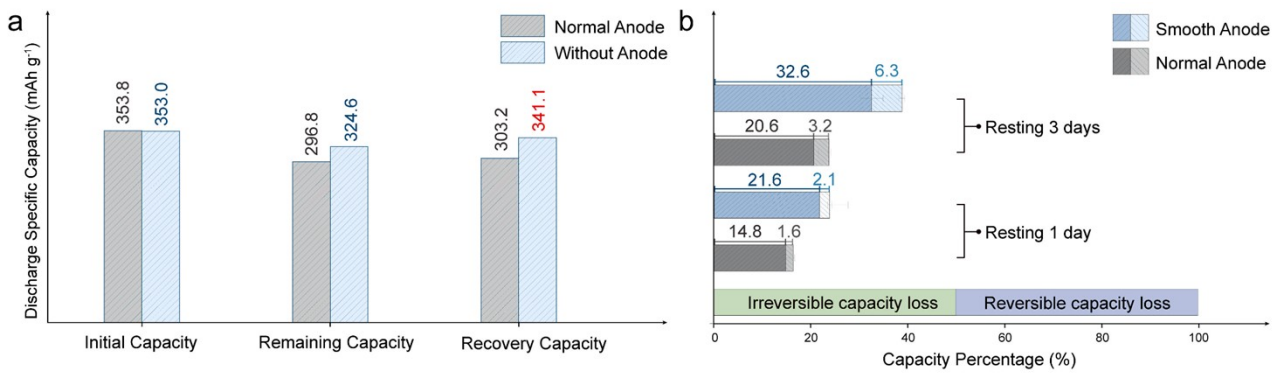


**Fig. S8. The effect of Zn anode corrosion in $Zn(OTf)_2$ electrolyte during self-discharge.** (a) Comparison of self-discharge with and without the presence of Zn anode in $Zn(OTf)_2$. (b) The influence of different corrosion conditions in $Zn(OTf)_2$ on self-discharge.

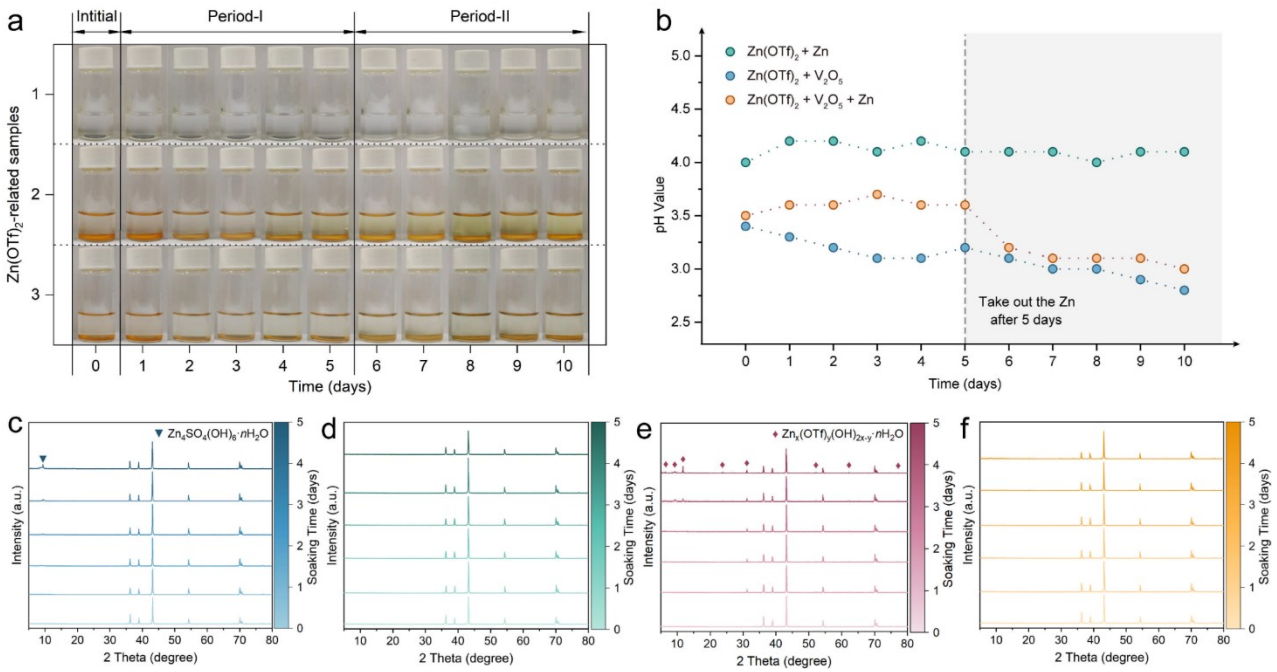


**Fig. S9. Immersion experiments on $Zn(OTf)_2$ and $ZnSO_4$.** (a) Immersion experiment in the $Zn(OTf)_2$ electrolyte. (b) Evolution of the pH values of the $Zn(OTf)_2$ electrolyte in the immersion experiment. (c) XRD of Zn without $V_2O_5$ in $ZnSO_4$*. (d) XRD of Zn with $V_2O_5$ in $ZnSO_4$. (e) XRD of Zn without $V_2O_5$ in $Zn(OTf)_2$[11, 12]. (f) XRD of Zn with $V_2O_5$ in $Zn(OTf)_2$.

**Notes*:** $Zn_4SO_4(OH)_6·3H_2O$ JCPDS No.39-0689, $Zn_4SO_4(OH)_6·4H_2O$ JCPDS No.44-0673.

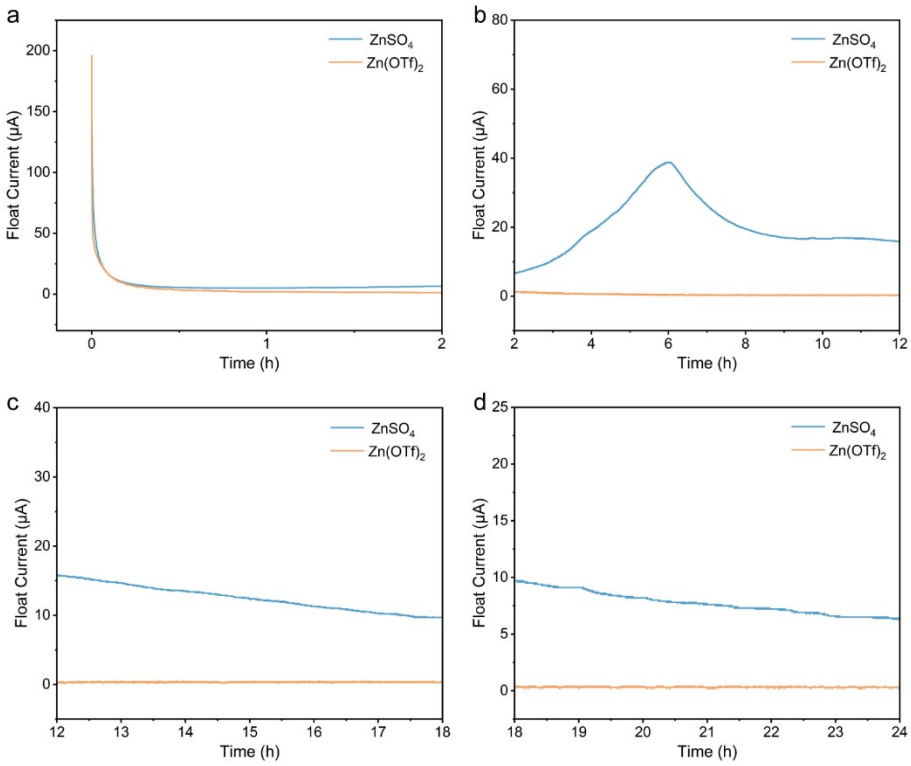


**Fig. S10. Detail of float current test of $ZnSO_4$ and $Zn(OTf)_2$.** (a) 0-2 h. (b) 2-12 h. (c) 12-18 h. (d) 18-24 h.

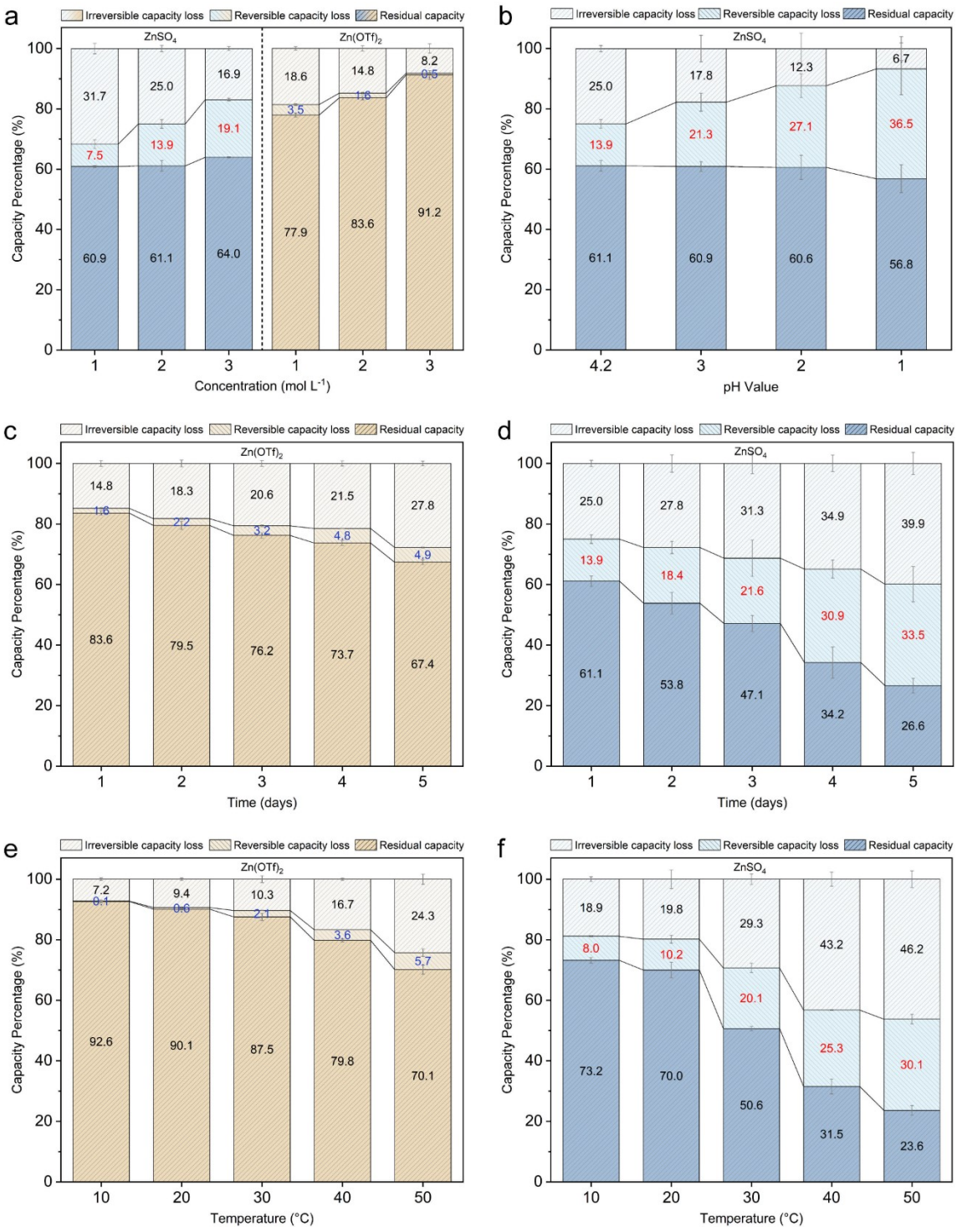


**Fig. S11 Regulating the impact of cell composition and test conditions on self-discharge.** (a) electrolyte concentration. (b) pH value. (c-d) Time. (e-f) Temperature.

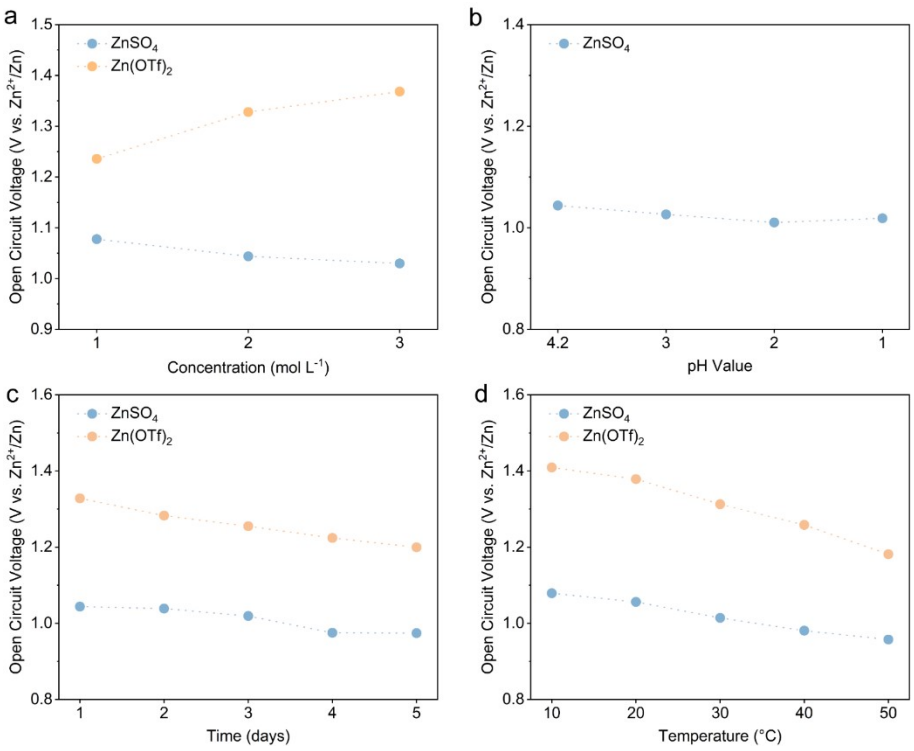


**Fig. S12. Open-circuit voltage after resting 24 hours under different configurations and test conditions.** (a) Concentration*. (b) pH Value. (c) Time. (d) Temperature.

**Notes*:** the open-circuit voltage is dependent on the SOC of the existing capacity, taking 3 M for example, let the capacity be 100, then the reversible capacity is 16.9, the reversible capacity is 19.1, and the residual capacity is 64.0, recovery capacity = reversible capacity + residual capacity. SOC: residual capacity/recovery capacity (64/(64+19.1))*100% = 77.02%, 1 M: 2 M: 3 M = 89.04%, 81.47%, 77.02%.

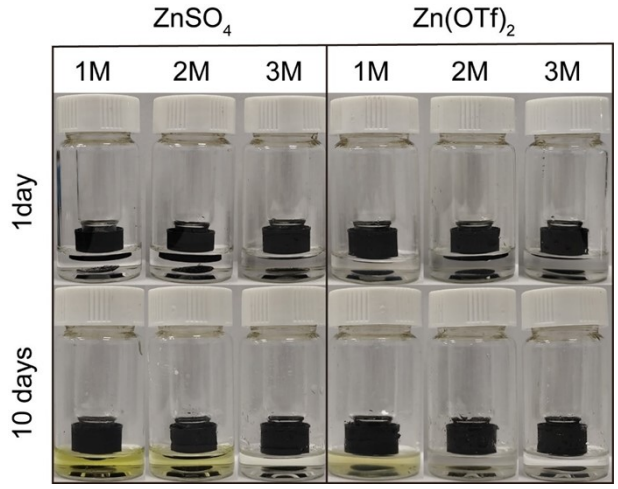


**Fig. S13.** Immersion experiment of Zn anode and $V_2O_5 \cdot nH_2O$ cathode at different concentrations of $ZnSO_4$ and $Zn(OTf)_2$ (Details as shown in **Fig. S21**).

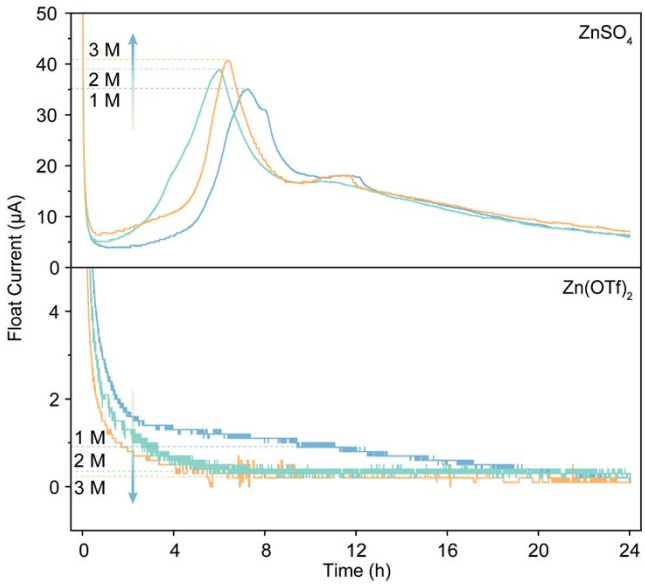


**Fig. S14.** Float current of $ZnSO_4$ and $Zn(OTf)_2$ cells with different electrolyte concentrations.

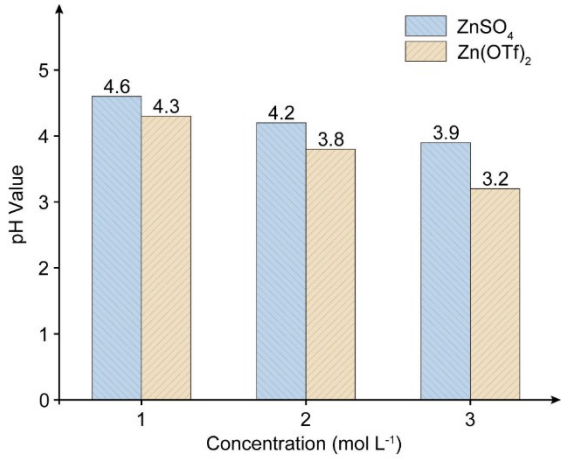


**Fig. S15.** The pH value of different concentrations of $ZnSO_4$ and $Zn(OTf)_2$ electrolytes.

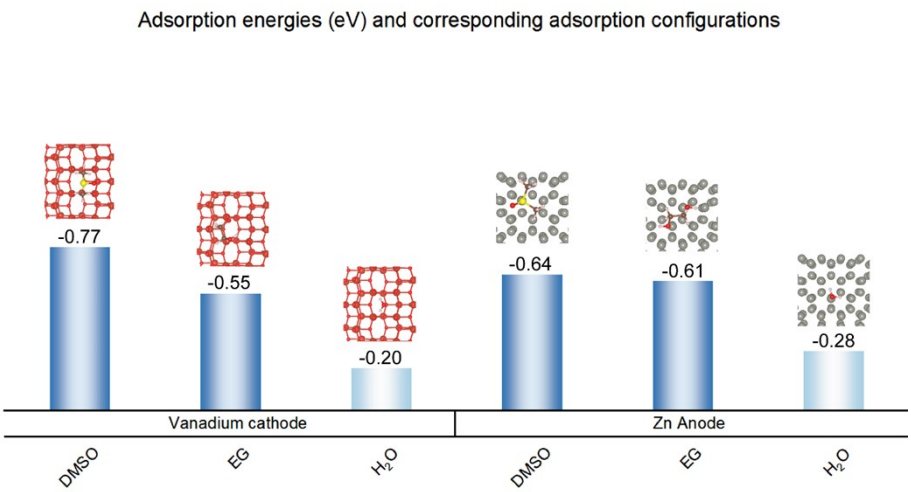


**Fig. S16.** Adsorption energies and corresponding adsorption configurations of DMSO, EG, and $H_2O$ on cathode and anode, respectively*.

**Note*:** The result shows that the adsorption energy of DMSO on the cathode is 0.77 eV, and for EG it is 0.55 eV, both higher than $H_2O$ on the cathode (0.20 eV). Similarly, the adsorption energies of these two additives on the anode side are 0.64 and 0.61 eV, respectively, both significantly higher than that of $H_2O$, which is 0.28 eV. This indicates that DMSO and EG can exclude the $H_2O$ molecules on the inner Helmholtz planes and occupy certain adsorption spaces of both cathode and anode, thereby reconfiguring the double electric layer and achieving the inhibition of vanadium dissolution and side reactions.

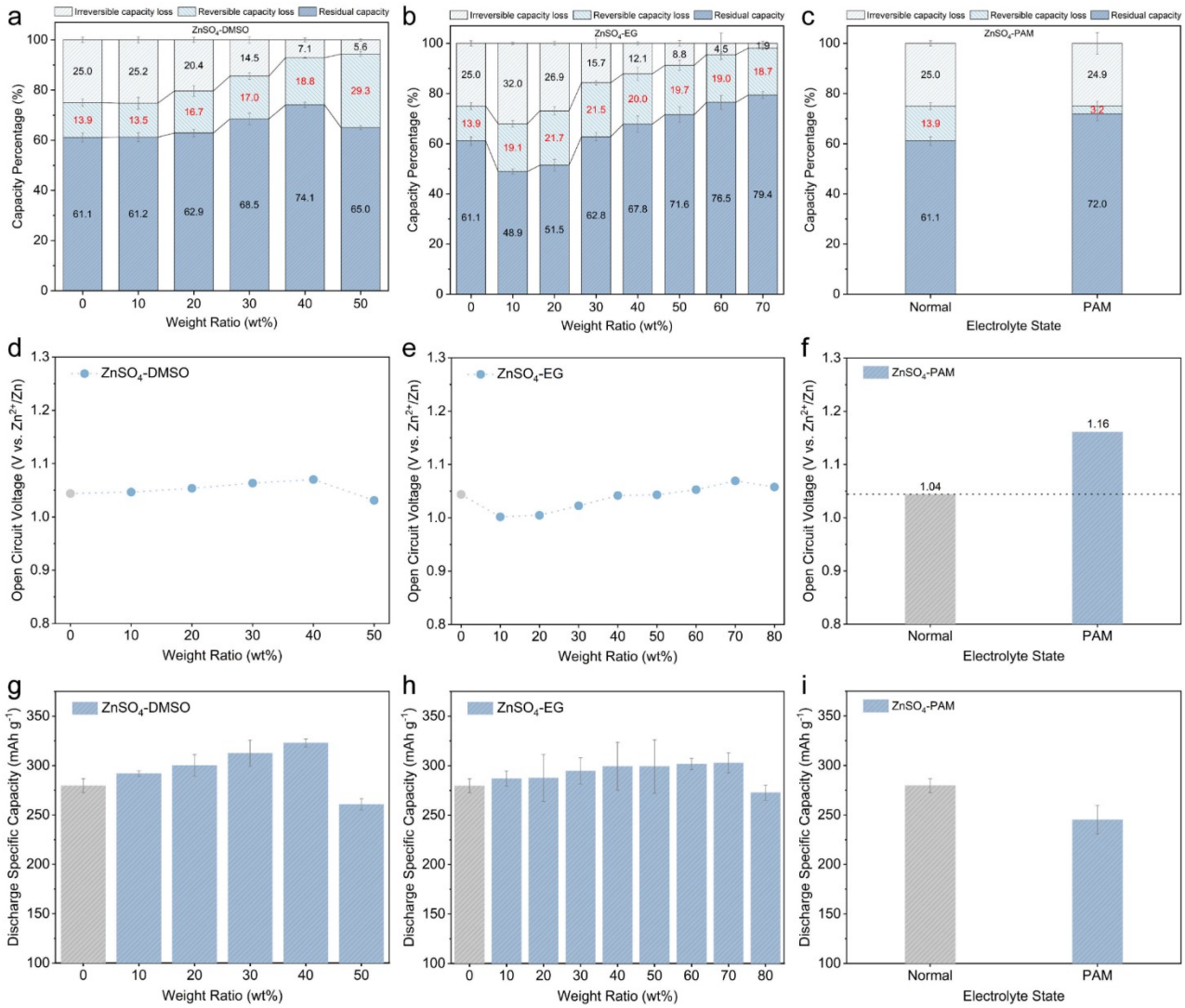


**Fig. S17. Self-discharge capacity percentage, open-circuit voltage, and initial capacity with different modifications.** (a-c) Self-discharge capacity percentage for $ZnSO_4$ with DMSO, EG, and PAM modifications. (d-f) 24-hour open-circuit voltage for $ZnSO_4$ with DMSO, EG, and PAM modifications. (g-i) Initial discharge capacity of the 2nd cycle of $ZnSO_4$ with DMSO, EG, and PAM modifications.

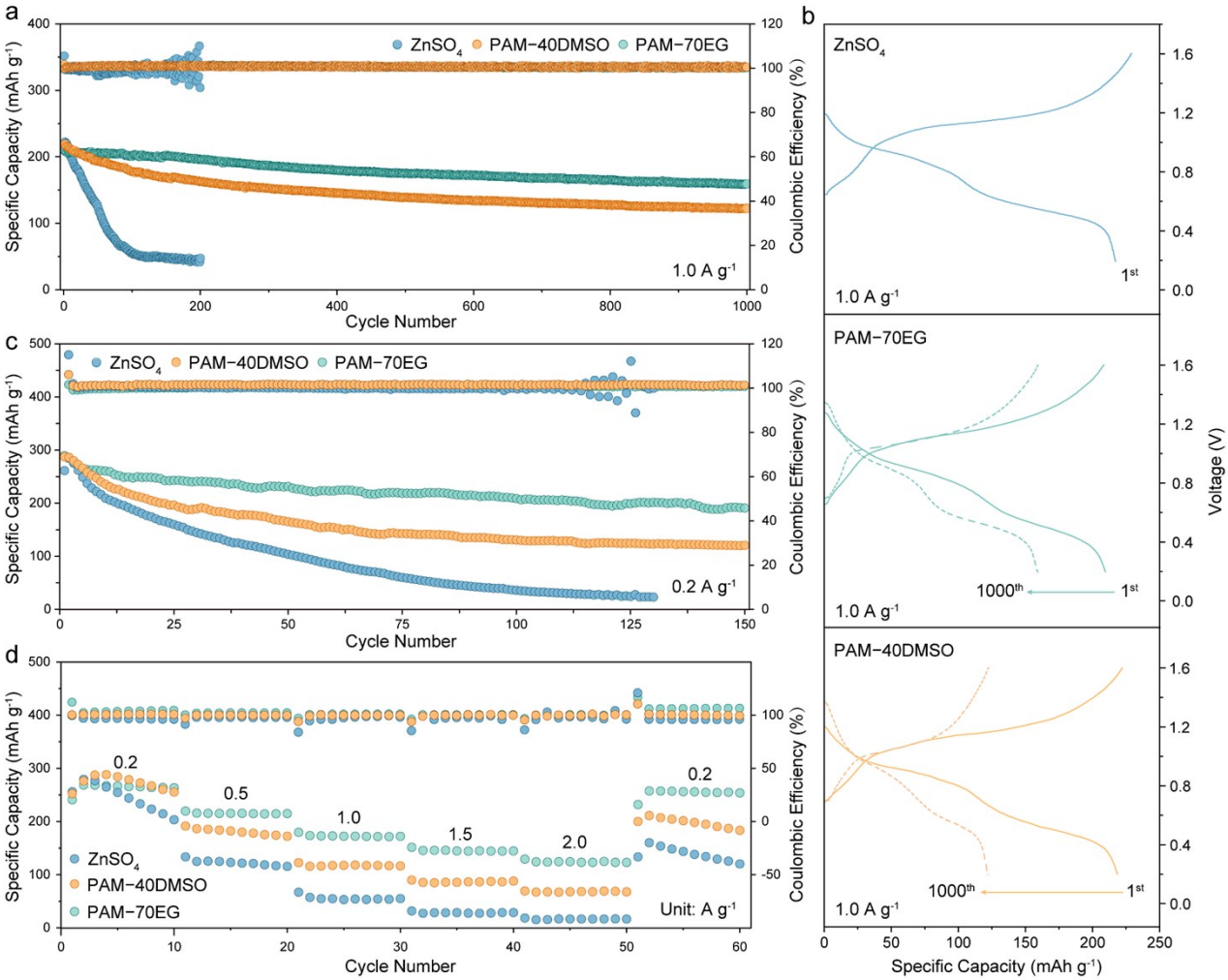


**Fig. S18.** The electrochemical performance of the Zn||$V_2O_5{\cdot}nH_2O$ cells using $ZnSO_4$, PAM-40DMSO, and PAM-70EG electrolytes. (a) Cycling performance at 1.0 A $g^{-1}$. (b) galvanostatic charge-discharge (GCD) profiles of the 1$^{st}$ and 1000$^{th}$ cycle at 1 A $g^{-1}$. (c) Cycling performance at 0.2 A $g^{-1}$. (d) Rate performance.

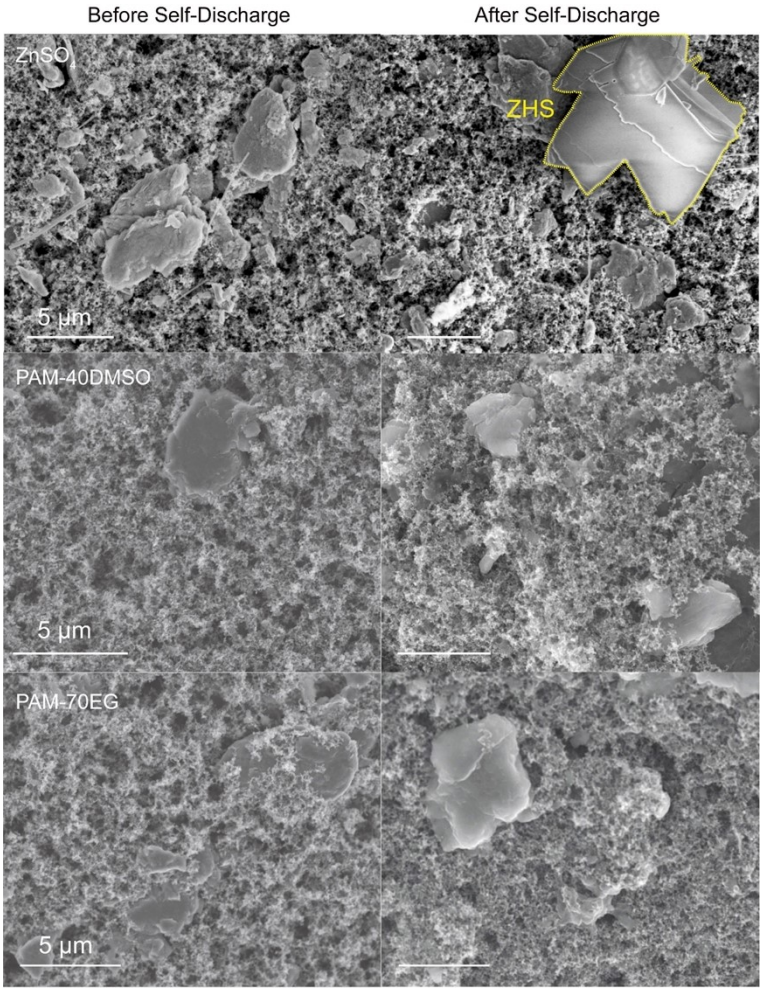


**Fig. S19.** The morphological changes of the cathode before and after self-discharge for $ZnSO_4$, PAM-40DMSO, and PAM-70EG electrolytes*.

**Notes*:** In the $ZnSO_4$ electrolyte, ZHS byproducts were observed at the cathode side after 24 hours of self-discharge. However, no significant by-products were found after self-discharge in the PAM-40DMSO and PAM-70EG electrolytes.

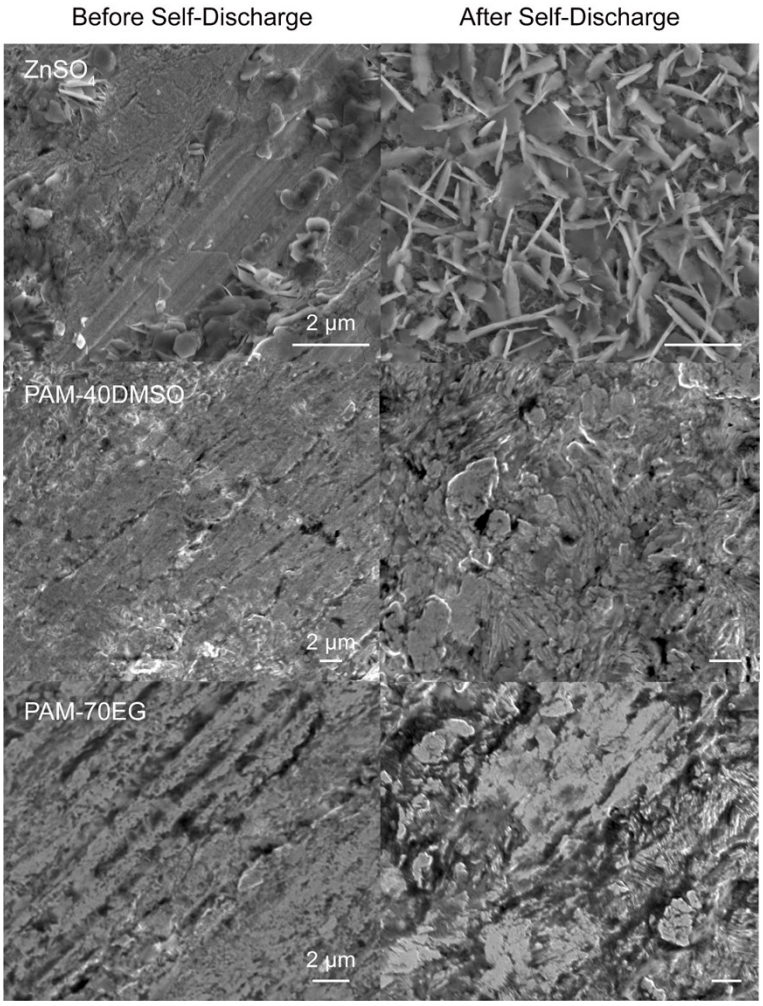


**Fig. S20.** The morphological changes of the anode before and after self-discharge for $ZnSO_4$, PAM-40DMSO, and PAM-70EG electrolytes*.

**Notes*:** In $ZnSO_4$ electrolyte, dense ZHS by-products were found on the anode side after 24 hours of self-discharge. Whereas, in PAM-40DMSO and PAM-70EG electrolytes, no significant by-products were observed after self-discharge.

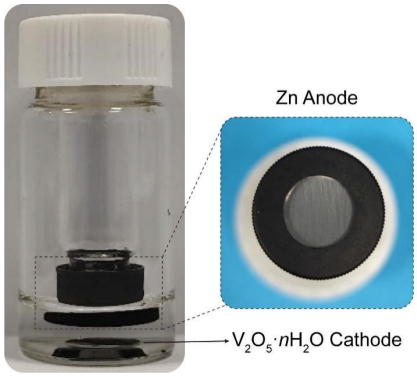


**Fig. S21.** Photograph of the immersion experiment.

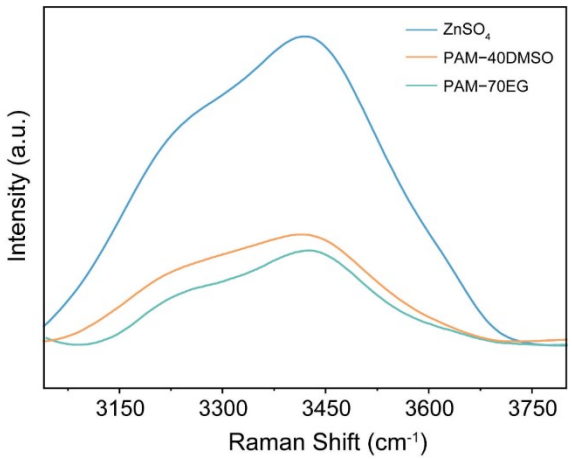


**Fig. S22.** Water activity test for $ZnSO_4$, PAM-40DMSO, and PAM-70EG electrolytes using Raman scattering*.

**Notes*:** The peaks at 3200–3700 $cm^{-1}$ in the Raman spectrum corresponding to the O–H stretching vibrational modes shifted to higher wavenumbers and the peak intensity was significantly reduced in PAM-40DMSO, PAM-70EG, suggesting that the interactions between $H_2O$ were weakened and the water activity was reduced[13].

Supplementary Notes.

**Note S1.** Self-discharge curve fitting[14, 15]

Ohmic leakage:

$$V = V_o e^{-\frac{t}{RC}} \quad \text{* MERGEFORMAT (1)}$$

where $V$ is the voltage at time (t), $V_o$ is the initial voltage, $R$ represents the ohmic leakage, and $C$ represents the capacitance.

Activation controlled:

$$V = V_o - \frac{RT}{\alpha F}\ln\frac{\alpha F i_o}{RTC} - \frac{RT}{\alpha F}\ln(t + \frac{CK}{i_o}) \quad \text{* MERGEFORMAT (2)}$$

where $R$ is the ideal gas constant, $T$ is the temperature, $\alpha$ is the charge transfer coefficient, $F$ is the Faraday constant, $i_o$ is the exchange current density, $C$ is the interfacial capacitance, and $K$ represents an integration constant.

Diffusion controlled:

$$V = V_o - C^{-1}2zF\cdot AD^{\frac{1}{2}}\pi^{-\frac{1}{2}}C_o\sqrt{t} \quad \text{* MERGEFORMAT (3)}$$

where $z$ is the charge number of the impurity ions, $A$ is electrode surface area, $D$ is a diffusion coefficient, and $C_o$ is the initial concentration of impurities.

By combining equations (1)-(3), the total equation is as follows:

$$V = V_o e^{-\frac{t}{RC}} - \frac{RT}{\alpha F}\ln\frac{\alpha F i_o}{RTC} - \frac{RT}{\alpha F}\ln(t + \frac{CK}{i_o}) - C^{-1}2zF\cdot AD^{\frac{1}{2}}\pi^{-\frac{1}{2}}C_o\sqrt{t} \quad \text{* MERGEFORMAT (4)}$$

Since the ohmic leakage is negligible making $e^{-\frac{t}{RC}}$ approximately equal to 1, $V_o e^{-\frac{t}{RC}}$ is nearly equal to $V_o$. By permuting $\sqrt{t}$ = x (t = $x^2$), the equation is therefore transformed as follows:

$$V = V_o - \frac{RT}{\alpha F}\ln\frac{\alpha F i_o}{RTC} - \frac{RT}{\alpha F}\ln(x^2 + \frac{CK}{i_o}) - C^{-1}2zF\cdot AD^{\frac{1}{2}}\pi^{-\frac{1}{2}}C_o x\ (x = \sqrt{t}) \quad \text{* MERGEFORMAT (5)}$$

The equation is further simplified as follows:

$$V = V_o + m\ln(x^2 + n) + kx + c \ (x = \sqrt{t})$$ *

MERGEFORMAT (6)

It can be observed that the voltage (V), tends to vary as a function of $\ln(x^2+n)$ with respect to activation control, and V tends to vary as a function of $kx$ with respect to diffusion control.

**Supplementary References**


1. G. Kresse, *Phys. Rev. B*, 1996, **54**, 11169-11118.
2. J. P. Perdew, K. Burke and M. Ernzerhof, *Physical review letters*, 1996, **77**, 3865-3868.
3. G. Kresse and D. P. Joubert, *Physical Review B*, 1999, **59**, 1758-1775.
4. V. Wang, N. Xu, J.-C. Liu, G. Tang and W.-T. Geng, *Computer Physics Communications*, 2021, **267**, 108033.
5. S. Grimme, J. Antony, S. Ehrlich and H. Krieg, *The Journal of chemical physics*, 2010, **132**, 154104.
6. Z. Moradi-Shahrbabak and M. Jadidoleslam, *IET Renewable Power Generation*, 2023, **17**, 1699-1712.
7. X. Jia, C. Liu, Z. Wang, D. Huang and G. Cao, *Nano-Micro Letters*, 2024, **16**, 129.
8. M. Li, Z. Li, X. Wang, J. Meng, X. Liu, B. Wu, C. Han and L. Mai, *Energ Environ Sci*, 2021, **14**, 3796-3839.
9. B. Lee, H. R. Seo, H. R. Lee, C. S. Yoon, J. H. Kim, K. Y. Chung, B. W. Cho and S. H. Oh, *ChemSusChem*, 2016, **9**, 2948-2956.
10. J. Zhang, J. Sun, D. Yang, S. Ha, T. Ma, H. Liu, X. Shi, D. Guo, Y. Wang and Y. Wei, *Nano Letters*, 2024, **24**, 688-695.
11. J. Hu, Y. Qu, F. Shi, J. Wang, X. He, S. Liao and L. Duan, *Adv Funct Mater*, 2022, **32**, 2209463.
12. P. Oberholzer, E. Tervoort, A. Bouzid, A. Pasquarello and D. Kundu, *ACS Applied Materials & Interfaces*, 2019, **11**, 674-682.
13. Y. Kang, F. Zhang, H. Li, W. Wei, H. Dong, H. Chen, Y. Sang, H. Liu and S. Wang, *ENERGY & ENVIRONMENTAL MATERIALS*, 2024, e12707.
14. B. E. Conway, W. G. Pell and T. C. Liu, *Journal of Power Sources*, 1997, **65**, 53-59.
15. J. J. Niu, B. E. Conway and W. G. Pell, *Journal of Power Sources*, 2004, **135**, 332-343.